Nanoarchitectonics of ethylene propylene diene monomer (EPDM) composites reinforced with Cu–Al–Zn-alloy for ultrasonic array transducers' fabrication

Mirham A. Y. Barakat[1] · **Salwa H. El-Sabbagh[2]** · **Wael S. Mohamed[2]** · **Doaa S. Mahmoud[2]**

Abstract

In response to the continuous demand for industry progress and the need for low-cost alternative materials that have superior properties than the present ones, a new coupling agent was used to treat composites, which were used as new backing materials in ultrasonic array transducers. In array transducers, back-echo reverberation to the piezoelectric elements occurs, so backing materials are critical in reducing these echoes. The Cu–Al–Zn-alloy was treated with a coupling agent before being incorporated into ethylene propylene diene monomer (EPDM) composites. Cu–Al–Zn-alloy/EPDM composites were assessed using rheometric, mechanical, and morphological properties. The division of cu-alloy at the EPDM matrix was visualized using a scanning electron microscope (SEM). TGA and DSC techniques were used to study the thermal characterization of the EPDM composites. As a result, the treated Cu-alloy improved the thermal, mechanical, and morphological characteristics of EPDM composites. Ultrasonic measurements ensured the composites' effectiveness as backing materials in ultrasonic array transducers. Furthermore, the composites' properties were similar to those of the most commonly used epoxy/tungsten backing material. Finally, linear ultrasonic-phased array transducers were fabricated using Cu–Al–Zn-alloy/EPDM composites. They had a low signal-to-noise ratio, and this ensured the effectiveness of Cu–Al–Zn-alloy/EPDM composites as backing materials.

Keywords Cu–Al–Zn-alloy · EPDM composites · Backing material · Ultrasonic array transducer

1 Introduction

An ultrasonic array transducer is one transducer that includes a piezoelectric element divided into a numeral of separately attached elements, which are surrounded by a polymer composite. It can take the shape of a 1D, a 2D or an annular. In recent years, the need for ultrasonic arrays for non-devastating valuation has increased greatly. Arrays could increase inspection quality in a shorter amount of inspection time. They have advantages over the traditional single-element transducers: one array can do a number of different searches,

and they are able to output instant images of the test frame. These merits promise many applications in the engineering industry. Therefore, broad range of research described array transducers and their risk capability [1]. Using a diamond wire saw, blocks of piezoceramic material, such as lead zirconate titanate (PZT-5 H), were cut into individual elements to create arrays. To lessen element-to-element cross-talk, the spaces between the elements can be filled with a loss polymer [2]. An ultrasonic array transducer is a good tool to envisage solids. They were primarily developed for medical discovery. They can also see the internal flaws in metals, which is useful in industrial settings. Some four-sided piezoelectric devices that can function as both transmitters and receivers make up a linear array transducer [3, 4].

A low-frequency (LF) array transducer is suitable for concrete inspection compared to a high-frequency (HF) array transducer for metal detection. Two basic challenges may arise during the manufacturing of an array transducer. The cross-talk between piezoelectric components is the first challenge. Crosstalk can produce a lot of noise and

✉ Mirham A. Y. Barakat
  mirham75@yahoo.com

1   Ultrasonic Metrology Department, National Institute of Standards, Giza Code 12211, Tersa Street, P O Box: 136, Haram, Giza, Egypt

2   Polymers and Pigments Department, National Research Centre, Giza, Egypt

hinder the ability to steer the beam, while it is being transmitted and received. This cross-talk is brought on by inadequate mechanical and electrical isolation between elements [5]. The second challenge is figuring out how to stop unwanted reverse energy from coming back to the piezoelectric components. The dampening of the piezoelectric elements' vibration after excitation is greatly aided by a backing layer that is bonded to them. A wider frequency bandwidth and higher axial resolution are the outcomes. Additionally, the backing layer dissipates the energy [6].

Since many years ago, the industrial sector has shown a great deal of interest in inorganic/elastomer composites with exceptional dielectric properties that also benefit from good flexibility, light weight, and simple production [7]. Researchers have recently become involved in Cu-based alloys memory shape (SMAs) because of its great shape memory capacity, narrow temperature region of transformation, and low manufacturing cost. As a result, Cu-based alloys can be utilized in a diversity of implementations, such as catalysis, electronics, as well as the production from metal matrix composites [8]. Composites of rubber and heavy metallic particles may be considered as an example of backing materials [9]. The backing material is important, because it prevents back echoes from reverberating to the piezoelectric element and reduces noisy echoes. Because (LF) low-frequency shakings are fewer attenuated than great-frequency (HF) vibrations, an LF array transducer should not have a backing layer. Due to the long-lasting reverberation in the backdrop layer, this can produce additional noise. This may cause additional noise due to the long-standing reverberation in the backing layer. As a result, when designing an HF array transducer, the backing layer plays an important part in inhibiting the vibration of each piezoelectric element after excitement and avoiding back wall echo reverberation [10]. The ability to dampen waves, prevent reverberation, and shorten back wall echoes are the main characteristics of such a backing material [11, 12]. Many researchers used ultrasonic techniques to investigate material properties [13, 14]. Additionally, Poisson's ratio, acoustic impedance, Lame's constants, and micro-hardness can be determined by the use of ultrasonic data [15, 16].

The purpose of this research was to look into the effects of Cu-alloy loading on the performance of Cu-alloy in EPDM composites intended for use in ultrasonic array transducers. Furthermore, the thermal stability, morphological, rheometric, and mechanical properties of Cu-alloy/EPDM composites are thoroughly investigated to support the effectiveness of Cu-alloy particles as reinforcing fillers. As a result, EPDM composites were ultrasonically measured to determine their suitability as backing materials for high-frequency array transducers.

2 Materials and experimental methodology

2.1 Materials preparation

Rubber made from EPDM (ethylene propylene diene). Produced by ESSO Chemie Germany, Vistalon 650S Diene (ethylidenenenorbornene) concentration is 9%, ethylene content is 55%, and the density is 0.86. The Mooney viscosity is ML (18) at 127 °C 48–52. CBS (*N*-Cyclohexyl-2-benzothiazole sulphenamide) is applied as an accelerator. It was supplied by Rheinehemie, Germany. At 15 °C, $C_{18}H_{32}O_2$ (stearic acid) and ZnO (zinc oxide) are used as activators, with specific gravity of 5.55–5.61 and 0.9–0.97, respectively. They were supplied by Aldrich Company, Germany. Elemental sulfur was supplied by Aldrich Company, Germany. TMQ (polymerized 2, 2, 4-trimethyl-1, 2-dihydroquinoline) is a commercial grade product. Used as an antioxidant. Cu-based alloy (Cu–Al–Zn-alloy) DEVARD`s Alloy Extra pure, LOBA CHEMIE PVT. LTD.

2.1.1 Preparation of coupling agent

Solution polymerization of 3-(Trimethoxysilyl) propyl methacrylate (TMSPM): To obtain poly 3-(Trimethoxysilyl) propyl methacrylate with a solid content of 20%, 3-(Trimethoxysilyl) propyl methacrylate (TMSPM) was solution polymerized in acetone solvent as follows: 20 ml of 3-(Trimethoxysilyl) propyl methacrylate monomer and 75 ml of acetone solvent were added to a 250 ml two-necked flask. The solution was bubbled with nitrogen for 30 min before being heated at 80 °C. Finally, 0.041 gm of AIBN (azobisisobutyronitrile) in 5 ml of acetone was added to the reaction. Poly 3-(Trimethoxysilyl) propyl methacrylate was formed after 4 h of polymerization reaction.

2.1.2 Preparation of EPDM composites

Different concentrations of untreated and treated Cu–Al–Zn-alloy at 2.5, 5, 10, 15, and 20 phr were mixed with EPDM and other components as stated by ASTM D3182-07(2012) standard in a two-roll mill, as shown in Tables 1, 2. The admixture rubbers were left overnight before vulcanization. The rheological characteristics of the blends containing Cu–Al–Zn-alloy were specified employing MDR One Moving Die Rheometer, TA at 152 ± 1 °C as stated by ASTMD2084-11, 2011. Materials structure, fabrication, and treatment are summarized in Scheme 1.

Table 1 Formulations and rheometric properties of the Cu–Al–Zn /EPDM/ composites

Ingredient phr/formula no	E0	E1	E2	E3	E4	E5	E6
Cu–Al–Zn	–	2.5	5	10	15	20	25
Rheometric characteristic at 152 ± 1 °C							
Scorch time (t_{S2}), min	5.13	7.18	1.78	1.67	1.59	1.57	1.41
Torque difference (ΔS), dN.m	13.73	13.99	11.91	11.57	10.88	10.48	10.55
Cure rate index (CRI), min-1	4.931	6.56	5.62	5.66	5.61	5.61	5.55
α_f	–	0.01894	− 0.1326	− 0.1573	− 0.2076	− 0.2367	− 0.2316

Table 2 Formulations and rheometric properties of the Cu–Al–Zn/EPDM in existence coupling agent

Ingredient phr/formula no	E0	E7	E8	E9	E10	E11	E12
Coupling agent	–	4	4	4	4	4	4
Cu–Al–Zn	–	2.5	5	10	15	20	25
Rheometric properties at 152 ± 1 °C							
Scorch time (t_{S2}), min	5.13	7.1	6.34	5.59	4.9	3.2	2.75
Torque difference (ΔS), dN.m	13.73	14.9	14.7	14.69	14.56	14.42	14.23
Cure rate index (CRI), min^{-1}	4.931	7.634	7.898	7.87	7.58	6.76	6.78
α_f	–	0.08521	0.0706	0.06992	0.06045	0.05025	0.03642

Base recipe (in phr): Ethylene propylene diene monomer (EPDM) 100; stearic acid 2; ZnO 5; CBS 1; Paraffin oil 2; S 3. TMQ 1; ΔS is the difference between M_H and M_L torque; CRI—cure rate index, α_f reinforcement factor, where phr is part per hundred parts of rubber

Scheme 1 Schematic of the fabrication process of Cu–Al–Zn /EPDM composites
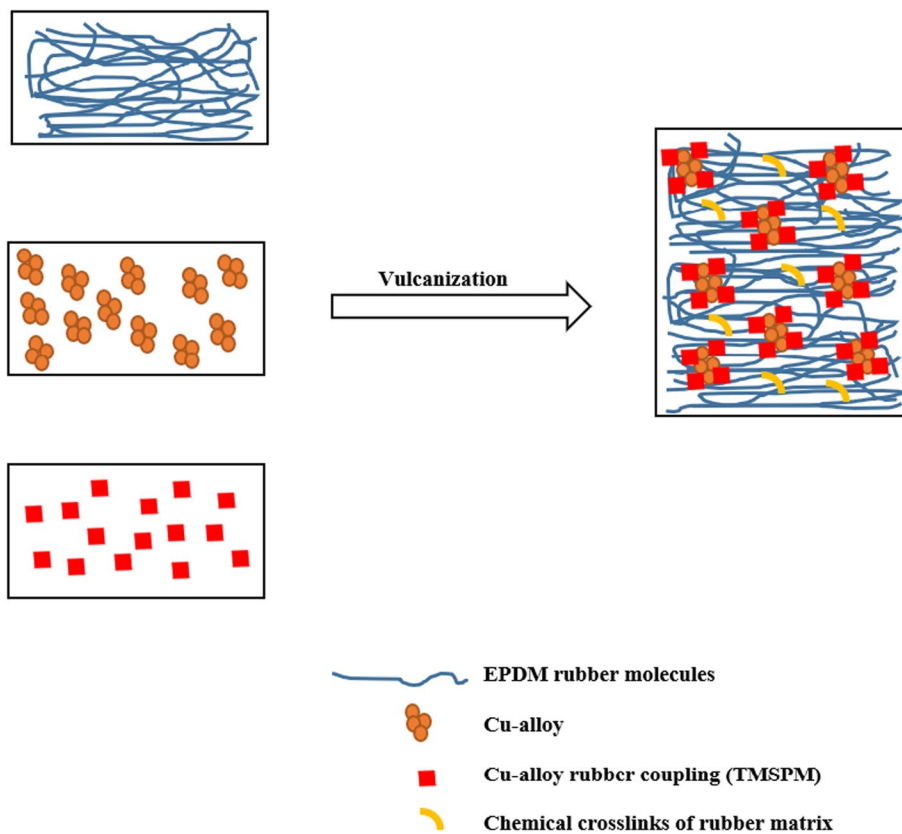
2.2 Morphology characterization

Using SEM to assessment the particle forms of Cu-alloy and the face homogeneity of EPDM vulcanizates without and with treated Cu-based alloy through utilizing microanalyzer electron probe (JEOL JX 840) (Japan). The Cu-alloy/EPDM specimens were photographed using SEM after the specimens were cover with a very fine layer of gold.

2.3 Thermal properties

The TGA (thermogravimetric analysis) was carried out applying Perkin Elmer analyzer equipment, USA. The samples were scanned from 50 to 1000 °C at a heating rate of 10 °C/min under nitrogen.

2.4 Differential scanning calorimeter

DSC analyses were carried out by SDT-Q600, USA, within a nitrogen atmosphere at heating rate of 10 °C/min from − 1.11 °C to 260 °C.

2.5 Rheometric characteristics

Rheometric characteristics of EPDM composites with different Cu–Al–Zn contents with connection agents TMSPM were measured by MDR One Moving Die Rheometer, TA Instruments, (New Castle, DE, USA) at 15 ± 1 °C in conformity with ASTM D2084-11.

2.6 Physical properties

Physical characteristic was performed in agreement with ASTMD412-06a (2013), using tensile testing machine Zwick Roell Z010 (Ulm, Germany). The hardness of prepared samples was specified utilizing the Shore A durometer as stated by ASTMD 2240. Fatigue testing was determined with Monsanto Fatigue.

2.7 Strain-energy determination

Simpson's rule was used to compute the strain energy [17, 18].

2.8 Ultrasonic measurement

Direct contact pulser receiver transducers use the through transmission technique as an ultrasonic mode of operation in accordance with the ASTM standard (ASTM E114-15, 2015 [19]) by direct contact pulser receiver transducers. Longitudinal normal beam ultrasonic transducers of 4 MHz (S12HB4, Karl Deutsch) and 2 MHz (S24HB4, Karl

Deutsch), in addition to a shear ultrasonic transducer of 2 MHz (S12Y2, Karl Deutsch), were used. The ultrasonic flaw detector (USN60, GE inspection technologies) had an A-scan display and gave distance/amplitude information, and the oscilloscope (LeCroy W, wave Jet 354A) displayed time/amplitude of the echoes. Standards blocks (VI and VII) were used as reference test blocks to calibrate thickness measurements. The measurements were carried out at an ambient room temperature of 25 °C ± 10 °C and a relative humidity of 45% ± 5%.

3 Results and discussion

3.1 Ultrasonic measurements

The main purpose of this research was to look into Cu–Al–Zn /EPDM composites for use in ultrasonic array transducers. Therefore, we must investigate some important properties of the prepared composite, such as ultrasonic velocities, acoustic impedance, ultrasonic attenuation coefficient, and mechanical properties. These properties are critical ones that reflect good knowledge about backing materials usefulness to be used for the manufacture of an ultrasonic transducer for a given application.
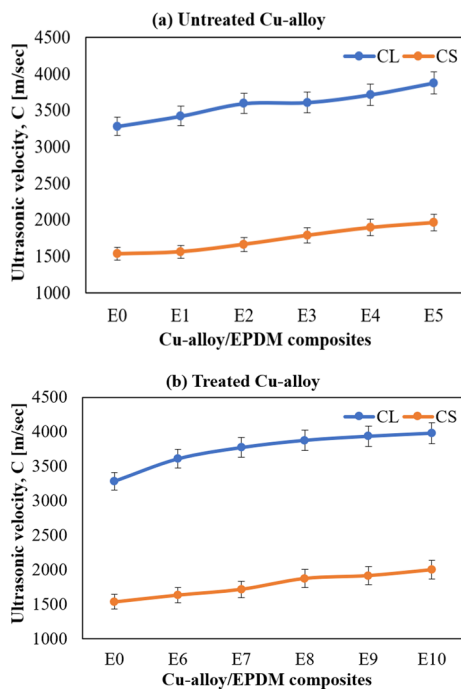
3.1.1 Ultrasonic velocities (C)

Ultrasonic velocities' measurements are found to be useful for investigating the material structure and the mechanical properties of the prepared EPDM composites. The main measured ultrasonic velocities are the longitudinal velocity and the shear one. Compressional waves are those with an ultrasonic longitudinal velocity. It is primarily determined by the specimen geometry in relation to wavelength. This is the most frequently velocity determined in laboratories, and it is directly related to a material's elastic properties. Shear waves are also referred to as transverse waves. The shear velocity is almost one-half that of longitudinal waves. Any materials that can support a shear wave can usually also support a longitudinal wave [20]. Ultrasonic velocities (longitudinal, C_L, and shear, C_S) were measured by the following formula [5], Fig. 1:

$$C = \frac{2x}{t}, \tag{1}$$

where C is the ultrasonic velocity, t is the time traveled by the echoes, and x is the thickness of the specimen.

Figure 1 shows that the ultrasonic velocities (longitudinal and shear) followed the same pattern, increasing with the increase in metal alloy. EPDM composites (E0 to E5) increased longitudinal velocities from about 3281 to 3876 m/s and shear velocities from about 1533 to 1963 m/s,

Fig. 1 The ultrasonic velocities (longitudinal, C_L and shear, C_S) for Cu-alloy/EPDM composites: (**a**) untreated Cu-alloy; (**b**) treated Cu-alloy

whereas EPDM composites (E6 to E10) increased longitudinal velocities from about 3281 to 3980 m/s and shear velocities from about 1533 to 1999 m/s. The treated Cu-alloy composites had higher velocities than the untreated ones.

We can conclude that increasing the alloy content in the EPDM matrix reduces intermolecular spacing and thus increases ultrasonic velocity [21], in addition the treatment of Cu/alloy caused further velocity increment. The alloy addition reduced the time required for the acoustic passage within the composite [22] and so did the treatment because of diminishing intermolecular spacing. As a result, the prepared EPDM composites will be good backing materials with good molecular arrangement and low intermolecular spacing, enhancing the absorption of unwanted back echoes from the piezoelectric material.

3.1.2 Acoustic impedance (Z)

The acoustic impedance (Z) is one of the important factors to evaluate the backing materials of the ultrasonic transducers. It is a function of both the material's density (ρ) and the material's ultrasonic velocity (C), Fig. 2

$$Z = \rho C. \tag{2}$$

First, the density, for the prepared EPDM composites, was measured directly using digital electronic balance with
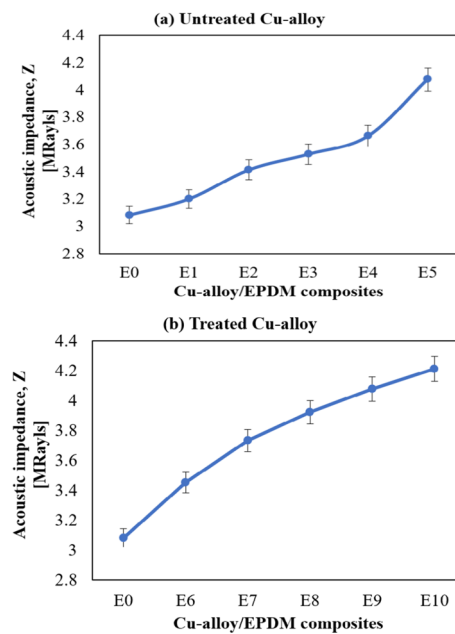
Fig. 2 The acoustic impedance (Z) for Cu-alloy/EPDM composites: (**a**) untreated Cu-alloy and (**b**) treated Cu-alloy

density determination kit; B150536815; Model MS2045; Mettler Toledo, Switzerland. Table 3 shows the density variation with different EPDM composites.

From Table 3, the density increased with different EPDM composites, until it reached its maximum at high alloy content. Because the alloy contains Cu, Al, and Zn, which are high-density metals, it filled the composite gaps and increased the mass. Furthermore, EPDM composites with coupling agents had a higher density than those without. The coupling agent increased the density; it was used in conjunction with the alloy to increase the mass of EPDM composites. To get a good backing material for array transducers, we need to get a material with a high density but not too dense, because the backing material for high-frequency array transducers needs to be effective at dampening the

Table 3 Density (ρ) for Cu/alloy EPDM composites

Specimen	Density (Kg/cm^3)
E0	0.94
E1	0.936
E2	0.95
E3	0.978
E4	0.986
E5	1.052
E6	0.957
E7	0.99
E8	1.012
E9	1.036
E10	1.058

excess vibration of the piezoelectric material without being too dense to completely prevent the piezoelectric material from moving. As a result, the prepared EPDM composites had appropriate densities for such a role, because the maximum density did not exceed 1.058 kg/cm^3.

Second, the acoustic impedance was calculated and Fig. 2 shows the variation of the acoustic impedance with the prepared Cu-alloy/EPDM composites.

The acoustic impedance increased with increasing alloy content in the EPDM matrix, reaching a maximum (4.08 MRayls) at E5 of 20 phr alloy content, as shown in Fig. 2a. Z increased by about 24% from E0 to E5. Furthermore, as presented in Fig. 2b, the acoustic impedance in the EPDM matrix increased with increasing treated alloy content until reaching a maximum of 4.2 MRayls at E10 of 20 phr treated alloy content. Z increased by about 26% from E0 to E10.

In general, the acoustic impedance (Z) describes the amount of resistance an ultrasonic beam encounters as it passes through a given material, i.e., it reflects the material's action to waves as a result of the material's structure [23]. Therefore, we can conclude that the resistance to wave flow increased as the alloy percentage increased in Cu-alloy/EPDM composites, as well as in composites containing a treated Cu-alloy. This ensures that the prepared composites may be good backing material for ultrasonic manufacture. They will enable good prevention of echo reverberation to the piezoelectric element, so the echo noise reduces and clear echo beam will be obtained.

In addition, the prepared EPDM composites with Cu–Al–Zn-alloy content could be considered as backing materials, because their acoustic impedance closely resembles the acoustic impedance of the epoxy with tungsten (Z_{epoxy} = 3 MRayls at 20 °C [24]) that was used as a good backing material for array transducers by many researchers. As a result, E0 (3.08 MRayls), E1 (3.2 MRayls), E2 (3.4 MRayls), E3 (3.5 MRayls), and E6 (3.45 MRayls) are the best prepared EPDM composites with Z close to that of epoxy with tungsten.

3.1.3 Ultrasonic attenuation coefficient (α)

Ultrasonic attenuation coefficient can provide useful information about the material structure of a given compound. The ultrasonic attenuation coefficient (α) calculated from two successive echo height measurements (l_1 and l_2) at distances x_1 and x_2, respectively. Figure 3 shows the ultrasonic attenuation coefficient of Cu-alloy/EPDM composites

$$\alpha = \left(1/(x_2 - x_1)\right)\left(\ln(l_1/l_2)\right) \tag{3}$$

From Fig. 3, the ultrasonic attenuation coefficient (α) ranged from about 1.7 to 2.04 dB/cm in EPDM composites
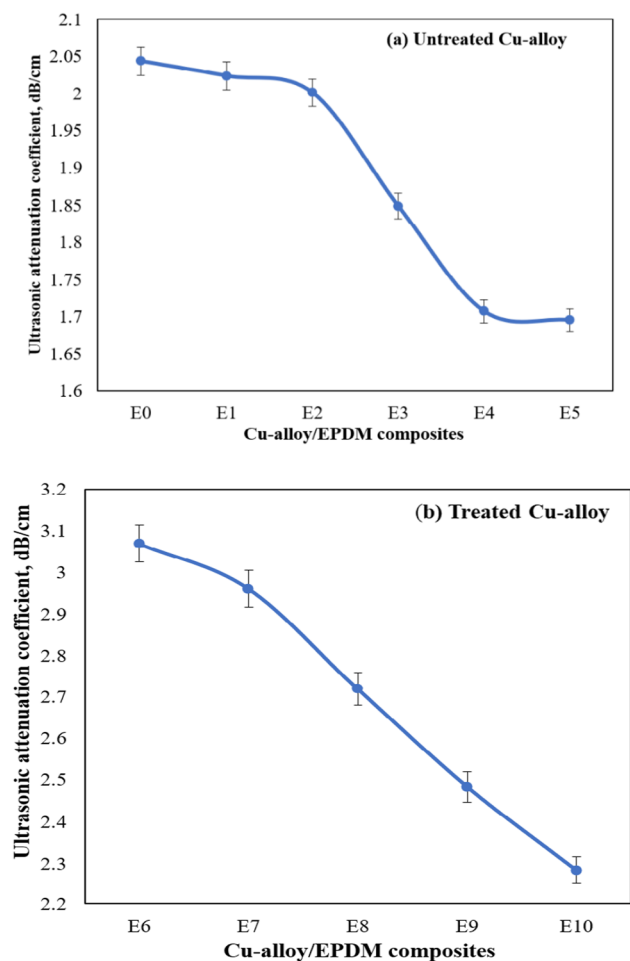
Fig. 3 The ultrasonic attenuation coefficient (α) for Cu-alloy/EPDM composites: (**a**) untreated Cu-alloy and (**b**) treated Cu-alloy

with untreated Cu-alloy, while it ranged from about 2.3 to 3.07 dB/cm in EPDM composites with treated Cu-alloy. The ultrasonic attenuation coefficient (α) reduced with the increment of Cu-alloy content in the EPDM matrix. Many studies have deduced that there is a linear relation between attenuation and material microstructure that includes defects, gaps, and so on. Consequently, the decrement in the ultrasonic attenuation coefficient demonstrated the decrement of defect or gaps in the prepared EPDM/Cu-alloy composites [23, 25]. This decrement ensures the well distribution of the Cu-alloy within the EPDM matrix with few gaps and imperfections between molecules. When making comparisons between the prepared EPDM composites and the epoxy with tungsten, we noticed that the most consistent composites were E6 (α = 3.07 dB/cm) and E7 (α = 2.96 dB/cm), because their ultrasonic attenuation coefficient (α) values were so close to that of epoxy with tungsten (α_{epoxy} = 3 dB/cm [24]).
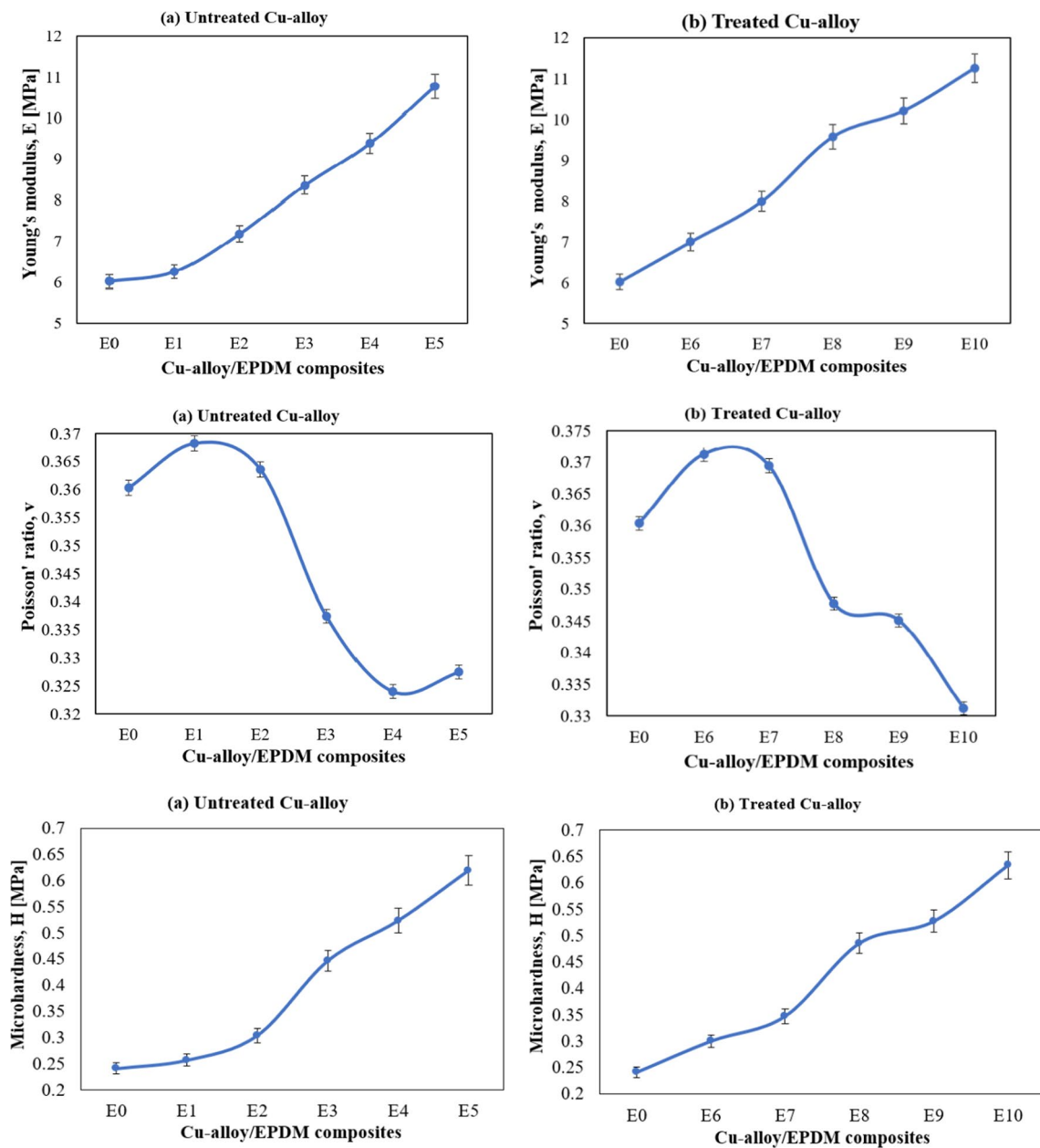
Fig. 4 Young's modulus (*E*), Poisson's ratio (*v*), and micro-hardness (H) for Cu-alloy/EPDM composites: (**a**) untreated Cu-alloy and (**b**) treated Cu-alloy

3.1.4 Mechanical properties by ultrasonic

The micro-hardness (*H*) and Young's modulus (*E*) were calculated to demonstrate some of the characteristics of the prepared EPDM composites and the influence of the alloy content [26] (Fig. 4). In addition, the mechanical properties of EPDM composites demonstrated their usefulness as backing materials

$$v = \frac{1 - 2\left(C_S/C_L\right)^2}{2 - 2\left(C_S/C_L\right)^2} \tag{4}$$

$$E = 2\rho(C_S)^2(1 + v) \tag{5}$$

$$H = [(1 - 2v)E/(6(1 + v)], \tag{6}$$

where v is the Poisson's ratio, ρ is the composite density, E is the Young's modulus, and H is the micro-hardness.

Figure 4a, b shows the variation of Young's modulus (E), Poisson's ratio (v), and micro-hardness (H) with the untreated Cu-alloy and the treated Cu-alloy. Young's modulus (E) and micro-hardness (H) increased from low content of untreated Cu-alloy (E0) to high content of untreated Cu-alloy (E5). Also, they increased from low content of treated Cu-alloy (E6) to high content of treated Cu-alloy (E10).

The Poisson's ratio calculated for EPDM composites decreased as the Cu-alloy content increased. The decrement of the Poisson's ratio ensured the improvement of the mechanical properties of the composites. We can say that the addition of treated Cu-alloy increased the mechanical properties [32]. The incorporation of 20 phr of treated Cu-alloy within the EPDM matrix significantly enhanced the mechanical properties of the composites.

As per the enhancement of the mechanical properties of the prepared composites, we may say that these composites will be good candidate as backing materials for array transducers. Especially, ultrasonic linear array transducers because the multiple piezoelectric elements need good impact soft backing materials to fill all gapes. In addition, they must be absorber of most back echoes that returned from the vibration of the multiple piezoelectric elements.

From the above characteristic properties of Cu-alloy/EPDM composites, we can notice the effectiveness of these composites as backing materials. They may have some advantages over the well-known epoxy with tungsten backing material (Table 4). Table 4 gives a brief comparison between the prepared Cu-alloy/EPDM composites and the epoxy with tungsten. The information about the epoxy with tungsten was collected from specified references.

As per previous research, typically, backing materials are composed of a polymer matrix, such as epoxy or polyurethane, and inorganic fillers of metallic particles, including tungsten, iron, copper, magnesium, and aluminum [29]. From Table 4, the characteristic properties of both Cu-alloy/EPDM composites and epoxy with tungsten are very similar, but Cu-alloy/EPDM composites may have a lower density and a higher ultrasonic velocity. This means that Cu-alloy/EPDM composites have a larger arrangement of intermolecular spacing, allowing the passage of waves easier.

In addition, they have a higher density that causes the inhibition of backwall echoes, but they are still soft enough to allow more movement of the piezoelectric material. The enhanced properties of Cu-alloy/EPDM composites will be proved in the coming sections of this work.

3.1.5 Ultrasonic transducer designing with the new prepared backing composites

The ultrasonic-phased array transducer was designed to be composed of multiple linear piezoelectric (PZT) elements, Cu-alloy/EPDM backing material, and parylene matching front layer (about 0.1 mm thickness), Fig. 5. The matching
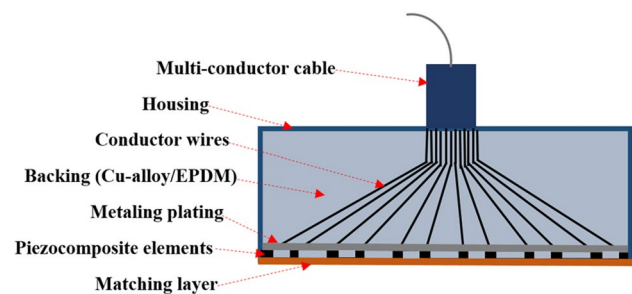
Fig. 5 Linear ultrasonic-phased array transducer with Cu-alloy/EPDM composites as backing material

Table 4 Cu-alloy/EPDM composites versus epoxy with tungsten

	Cu-alloy/EPDM composites	Epoxy with tungsten
Acoustic impedance, Z (MRayls)	3.08 to 4.2	3 [12–24]
Ultrasonic attenuation coefficient, α (dB/cm)	1.7 to 3.07	3 [30]
Density, ρ (Kg/cm³)	0.94 to 1.058	1.26 to 4 [27]
Ultrasonic velocity, C_L (m/s)	3281 to 3980	3146 [28]
Cost and availability	Relatively low cost and easy to prepare, composites have a longer lifespan than other products, saving money in the long run. They also have good solid abrasion and tear resistance	Relatively low cost and easy prepared composite [28]
Efficiency as backing material	Good impact soft backing material, good molecular arrangement with low intermolecular spacing, more enhanced mechanical and physical properties, and high dampen of noise echo	Good impact backing material, good molecular arrangement with intermediate intermolecular spacing, good mechanical and physical properties, and good dampen of noise echo [12–28]

layer is mainly for protection and to overcome the acoustic impedance mismatch between the piezoelectric element and the material under test. As per many researchers, parylene is good matching layer of very low acoustic impedance about 2.75 MRayls. The metallic plating is for connecting the piezoelectric elements together, and then, the conductor wires emerged from each element are collected to the multi-conductor cable. Cu-alloy/EPDM backing material fills the back space after the piezoelectric elements and the spaces between them. Thus, ten different linear ultrasonic-phased array transducers were fabricated. They contained Cu-alloy/EPDM composites (E0, E1, E2, E3, E4, E5, E6, E7, E8, E9, and E10).

3.1.6 Signal-to-noise ratio measurements

To assess the different prepared Cu-alloy/EPDM composites as backing materials, we measured the signal-to-noise ratio (S/N) from the different designed ultrasonic-phased array transducers that contain different Cu-alloy/EPDM composites as backing materials. The signal-to-noise ratio (S/N) could influence the test measurements of any designed transducer. S/N is affected by the specimen density (ρ), the ultrasound velocity in the specimen (C), beam width (BW), time interval (Δt), echo amplitude (A), and noise echo (N) [30]. It was presented in Table 5

$$S/N = \left(\sqrt{\frac{16}{\rho CBW\Delta t}} \right) \frac{A}{N}. \tag{7}$$

Using a vector signal analyzer (89441A-hp), the transducer spectrum chart (at -6 dB drop) was recorded, and then, the beam width (BW) was determined

Table 5 Signal-to-noise ratio of ultrasonic-phased array transducers that contain different Cu-alloy/EPDM composites as backing materials

Specimen	BW(MHz)	$\Delta t(\mu s)$	A/N	S/N
E0	2.7	0.2	0.6	0.058
E1	2.4	0.15	0.5	0.069
E2	2.5	0.11	0.6	0.102
E3	2.6	0.1	0.2	0.035
E4	2.2	0.09	0.35	0.077
E5	2.1	0.078	0.18	0.043
E6	2.5	0.12	0.12	0.018
E7	2.1	0.14	0.34	0.049
E8	2.2	0.13	0.5	0.071
E9	2.4	0.1	0.3	0.049
E10	2.1	0.12	0.24	0.036

$$BW = 100\frac{(f_u - f_l)}{f_o}, \tag{8}$$

where f_l is the lower frequency, f_u is the upper frequency, and f_o is the central frequency.

The time interval (Δt), echo amplitude (A), and noise echo (N) were determined using the flaw detector (USIP20, Krautkramer).

As shown in Table 5, the S/N values are very low, and they varied from about 0.018 to 0.1. The lowest value of S/N is recorded when using transducer with E6 backing composite. While, the highest one is for transducer with E2 backing composite. In general, we can say that the added backing composites were very effective to reduce noise echoes, but the most effective backing composite was E6. As per previous discussed results, E6 has the most consistent properties, such as acoustic impedance, ultrasonic attenuation coefficient, mechanical properties, etc., as the epoxy with tungsten backing material.

3.2 Morphology description

Cu-alloy/EPDM composites are thoroughly investigated to support the effectiveness of Cu-alloy particles as reinforcing fillers. SEM was utilized to determine the dispersion state of Cu-based alloy in EPDM composites, and also, the outcomes are presented in Fig. 6. An uneven together with ragged surface was observed for composite E0 (narrow holes). The particles are unequally distributed within the rubber matrix at lower concentrations of untreated and treated Cu-alloy (10 phr). Cu-alloy particles are found to be uniformly dispersed in the EPDM matrix at a high concentration of filler Cu-alloy 20 phr. The main reason for the uniform morphology and increased effective surface area for interacting with the rubber chains is the use of high concentrations of Cu-alloy with TMSPM (a coupling agent). The E3 composite exhibited agglomeration of untreated Cu-alloy. It is also clear that the high loading of untreated and treated Cu-alloy has a similar disparity in the EPDM matrix, as seen in composites E5 and E11, where the Cu-alloy forms aggregations. TMSPM-treated Cu-alloy particles, on the other hand, had a smaller size and a lower number of agglomerates in composite E9. It shows that treating Cu-alloy with the coupling agent (TMSPM) improves its dispersion in the EPDM matrix [8].

3.3 Thermal gravimetric analysis

Figure 7a, b shows the TGA thermograms of Cu-alloy/EPDM composites, as well as their derivative weight curves; the initial thermal degradation temperature (T_{onst}), which indicates the crest onset heat of degradation, and the final degeneration temperature (T_F), Furthermore, the degradation

**Fig. 6** SEM pictures of EPDM composites with untreated (E0, E3, and E5) and treated Cu-alloy (E9 and E11)
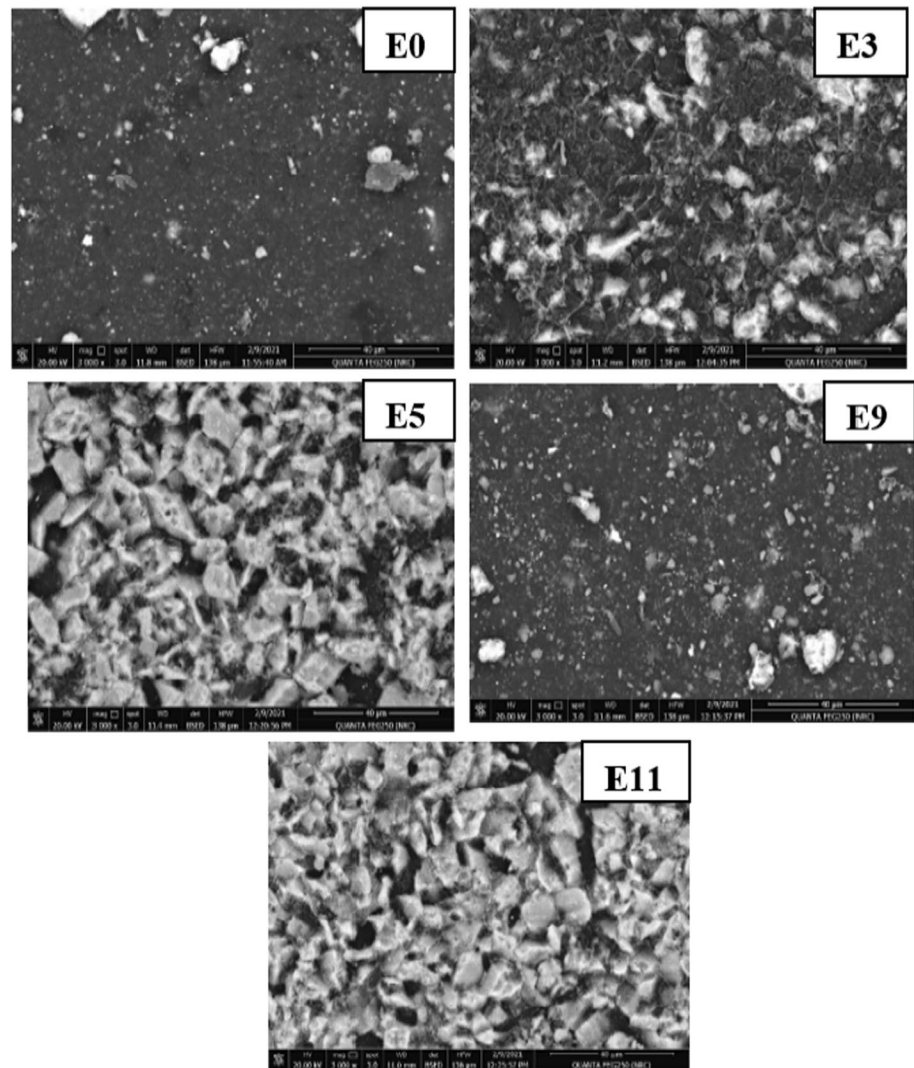
heat at 50% weight damage (T_{50}) is considered toward be a thermal stability index for rubber composites, and a temperature of 10% mass loss of sample ($T_{10}\%$) was taken as the beginning of decomposition. TGA graphs of E3, E5, E9, and E11 code samples containing untreated and treated Cu-alloy are shown in Fig. 7.

EPDM thermal decomposition occurs in two stages; the slight weight loss for EPDM composites at low temperatures is due to the volatilization of small molecular ingredients in all samples, while the main weight loss is due to the scission of cross-linked EPDM. As shown in Table 6, the degradation resistance of EPDM composites increased with the addition of Cu-alloy. The incorporation of 20 phr treated Cu-alloy resulted in a higher value of T_{onst} (onset degradation temperature of decomposition) than the other ratios of 10 and 20 phr untreated Cu-alloy. The uniform dispersion and interaction of Cu-alloy and EPDM matrix in the presence of TMSPM is attributed

to this result. Because of the good dispersion of treated Cu-alloy within the Cu-alloy/EPDM matrix, the rubber chain's thermal motion was restricted and heat distribution was uniform throughout the matrix [31]. It is also worth noting that the addition of 20 phr treated Cu-alloy resulted in a shift in the TGA peak (T_{50}) to higher temperatures, from 326 °C to 476 °C, and higher than the use of untreated Cu-alloy, indicating that vulcanized EPDM has improved thermal stability. Cu-alloy appears to have significantly improved thermal decomposition resistance, as evidenced by increasing T_{50}, indicating good heat resistance and restriction of polymer chain mobility imparted by the alloy particles.

The residual weight of Cu-alloy/EPDM composites containing 20 phr of treated Cu-alloy was greater than that of the other composites due to thermal stability improvement and the good interaction between Cu-alloy and EPDM matrix in the presence of TMSPM (Table 6).
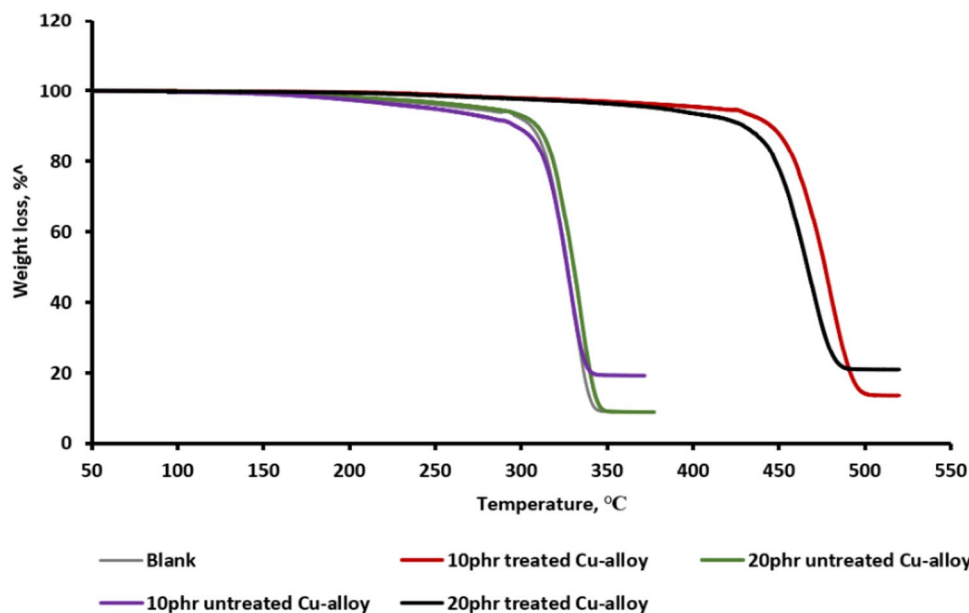
a TGA thermogram of the for EPDM loaded with untreated and treated Cu-alloy
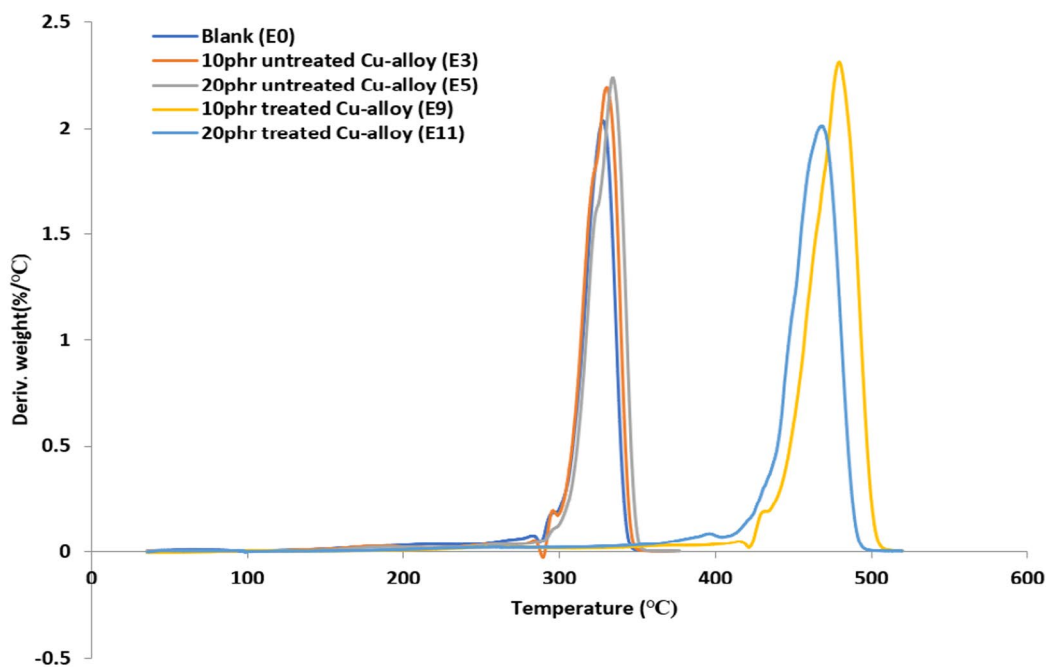
b Derivative thermogravimetric (DTG) curves for EPDM loaded with untreated and treated Cu-alloy

Fig. 7 **a** TGA thermogram of the EPDM loaded with untreated and treated Cu-alloy. **b** Derivative thermogravimetric (DTG) curves for EPDM loaded with untreated and treated Cu-alloy

3.4 Differential scanning calorimeter

The specific calorimetric data obtained from the DSC curves are presented in Tables 7, 8, 9. The peak melting temperatures of the EPDM composite phase increased as the Cu-alloy content increased, indicating a high level of EPDM crystal perfection. The peak temperature of crystallization in neat EPDM was 57.679 °C. In the absence of a coupling agent, the addition of Cu-alloy to EPDM resulted in a clear shift of the crystallization peak toward a high temperature. The crystallization peak temperature of the composites was shifted from 57.689 to 445 °C by the addition

Table 6 Thermogravimetric analysis (TGA) data for EPDM loaded with untreated and treated Cu-alloy

Codes of samples	T_{onst} °C	T_{10} °C	T_{30} °C	T_{50} °C	T_F °C	Peak temp. T_{max} (°C)	Residual weight (%)	Degradation rate (% min/°C)
Blank (E0)	272	303	319	326	374	475	9.06	437.06
10phr untreated Cu-alloy (E3)	280	293	319	326	371	475	13.58	434
20phr untreated Cu-alloy (E5)	396	307	322	330	377	476	9.038	438
10phr treated Cu-alloy (E9)	388	443	465	466	543	466	19.24	444
20phr treated Cu-alloy (E11)	415	425	455	476	519	468	20.95	437

T_{onst} is the onset temperature of degradation, T_{10}, T_{30} and T_{50} are the 10%, 30%, and 50% weight loss, and T_F is the final decomposition temperature that corresponds to the temperature after which there is negligible weight loss

Table 7 Data derived from the EPDM rubber composites' DSC curves (first heating scan)

Codes of samples	Tm_1 (°C)	ΔHm_1 (J/g)	Tcr_1 (°C)	ΔHcr_1 (m/v)	Tcc_1 (°C)	h_1 (°C)	Onset$_1$ (°C)	Offest$_1$ (°C)
Blank (E0)	151.98	274.1	57.689	− 9.849	39.37	39.37	39.52	143.45
10phr untreated Cu-alloy (E3)	328.56	2.02	321.72	− 1.18	314.84	314.84	317.8	325.88
20phr untreated Cu-alloy (E5)	456.18	32.36	445.22	− 1.82	405.84	405.84	412.26	454.6
10phr treated Cu-alloy (E9)	259.3	7.38	246.6	− 3.23	240.2	240.22	240.77	250.78
20phr treated Cu-alloy (E11)	128	211	41.56	− 7.1	28.34	28.34	25	117.66

Table 8 Data derived from the EPDM rubber composites' DSC curves (second heating scan)

Codes of samples	Tm_2 (°C)	ΔHm_1 (J/g)	Tcr_2 (°C)	ΔHcr_1 (m/v)	Tcc_2 (°C)	h_2 (°C)	Onset$_2$ (°C)	Offest$_1$ (°C)
Blank (E0)	453.98	52.6	440	− 5.17	405.59	405.59	408.72	451.8
10phr untreated Cu-alloy (E3)	450.71	23.084	424.2	− 2.28	392.27	392.27	408.6	448.88
20phr untreated Cu-alloy (E5)	507.9	157.44	474	− 10.76	455.8	455.7	457.8	498.8
10phr treated Cu-alloy (E9)	510.7	185.13	475.98	− 16.24	440.83	440.83	441.9	503
20phr treated Cu-alloy (E11)	459.65	157.09	468.7	− 8.72	406.3	406.3	434.3	490.9

Table 9 Data derived from the EPDM rubber composites' DSC curves (third heating scan)

Codes of samples	Tm_2 (°C)	ΔHm_1 (J/g)	Tcr_2 (°C)	ΔHcr_1 (m/v)	Tcc_2 (°C)	h_2 (°C)	Onset$_2$ (°C)	Offest$_1$ (°C)
Blank (E0)	504.7	155.58	474.99	− 15.57	457.07	453.8	457.07	498.21
10phr untreated Cu-alloy (E3)	504.46	96.91	478.12	− 11.29	450.91	450.91	457	499
20phr untreated Cu-alloy (E5)	588	5.3	585.16	− 1.47	576.73	576.73	577.48	588
10phr treated Cu-alloy (E9)	576.5	0.913	571.52	− 0.996	566.6	566.6	569	574.3
20phr treated Cu-alloy (E11)	591.69	16.76	586.14	− 3.11	570	570	571.8	590.2

h_1 is the first heating scan, h_2 is the second heating scan, and h_3 is the third heating scan, Tm_1 is the melting temperature recorded on the first heating scan, Tm_2 is the melting temperature recorded on the second heating scan, Tm_3 is the melting temperature recorded on the third heating scan, T_{cr} is the crystallization temperature, T_{cc} is the cold crystallization temperature, ΔHm_1 is the enthalpy of the melting profile recorded on the first heating scan, ΔHm_2 is the enthalpy of the melting profile recorded on the second heating scan, ΔHm_3 is the enthalpy of the melting profile recorded on the third heating scan, and ΔHcr is the crystallization enthalpy

of 10 or 20 phr of untreated Cu-alloy. The addition of 10 phr treated Cu-alloy increased the crystallization peak temperature of EPDM. In the first heating scan, the peak melting temperatures and the crystallization peak temperature of 20 phr treated Cu-alloy/EPDM composite were lower than those of neat EPDM. EPDM is affecting the movement and rearrangement of the EPDM molecular chains, resulting in the imperfect crystals. Furthermore, the Tm and
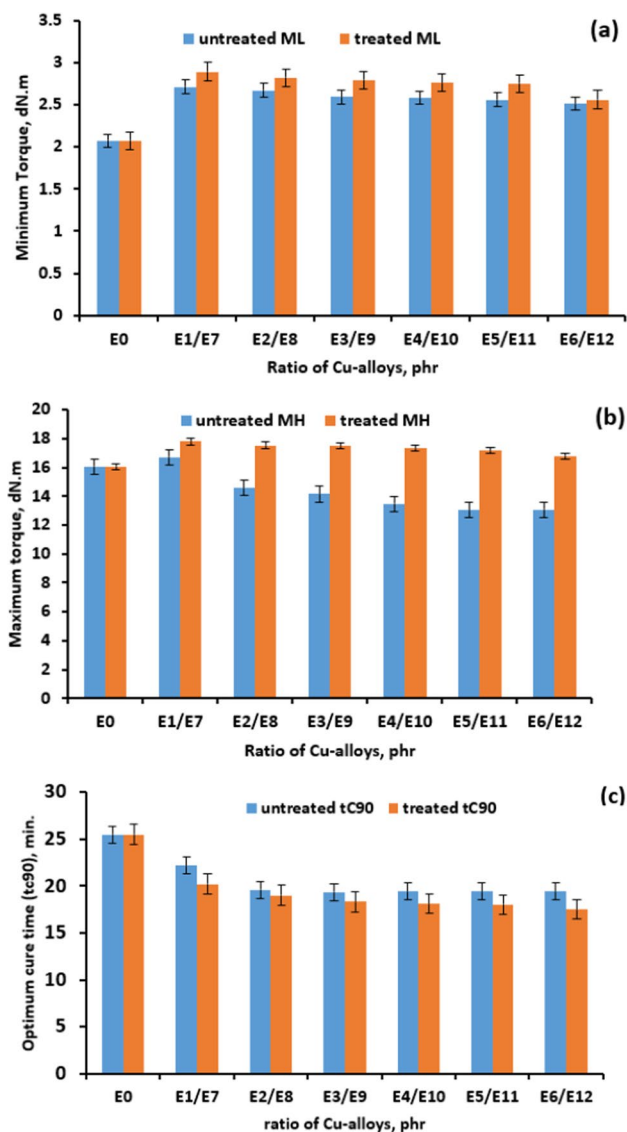
Fig. 8 Rheometric properties of EPDM composites loaded with untreated and treated Cu-alloy: (**a**) minimum torque; (**b**) maximum torque and (**c**) optimum cure time

Tcr values increased at treated Cu-alloy, accompanied by a decrease in melting (ΔHm) and crystallization enthalpies (ΔHcr). The cross-linking process reduces the crystalline phase during treatment (this result agrees with the data of difference torque). The cold crystallization transitions (Tcc) that are observed on all first heating runs are seen to be shifted toward a higher temperature range, demonstrating an increase in the percentage of amorphous macromolecules.

3.5 Rheological properties of Cu-alloy/EPDM composites

Tables 1, 2 and Fig. 8 show the rheological properties of EPDM filled with Cu-alloys, respectively. The minimum

torque (ML) is used as a measure of Cu-alloy-Cu-alloy inter-aggregate formation and also reflects the compounds' minimum viscosity [8]. Observed that the minimum torque rose initially by Cu-alloy filling and then decreased slightly. The value of ML is lower in the absence of a coupling agent than in the presence of TMSPM as conjunction agent. Higher value, stronger Cu-alloy–Cu-alloy interaction, resulting in a higher compound viscosity. Incorporating this Cu-alloy into EPDM compounds increased the filler–filler interaction, causing in a higher glueyness and improved processability from the Cu-alloy-filled EPDM compounds (as shown in Fig. 8). Maximum torque (MH) denotes the cross-link density of the vulcanized rubber.

In the existence of conjunction agent, the value of MH is greater than in the absence. Without conjunction agents, it can be seen that ΔS decreases with increasing Cu-alloy concentrations. In the presence of TMSPM, the values of ΔS are roughly the same. Rheometric torque changes with Cu-alloy filling can be used to describe the Cu-alloy/EPDM reaction or strengthening. The strengthening factor α_f can be counted from the rheography [32] and is given via

$$\alpha_f = \frac{\Delta T_{filled} - \Delta T_{gum}}{\Delta T_{gum}}, \tag{9}$$

where ΔT_{filled} is the torque difference in amount of filled composite and $\Delta T gum$ are the torque difference in value of unfilled/gum composite through vulcanization for the loaded and gum composite, respectively. Tables 1 and 2 contain values αf; it is obvious that the amounts of αf treated and untreated are constantly decreasing with the addendum of Cu-alloy. It notes that, the value of α_f in presence of TMSPM is higher than in absence. For high reinforcing efficiency purposes, raise EPDM–Cu-alloy reaction achieved, which was affected by the degree of filler dispersal. This may be owing to the striped option of the littlest particle sizes to make-better physico-mechanical properties. It is clear from Tables 1 and 2 that the CRI at first (2.5 phr of Cu-alloy) increased, and then, it is almost stable with rising the Cu-alloy content. It concluded that, at a comparable loading, treated Cu-alloy caused a rise α_f of filler. This was owing to best dispersal of Cu-alloy and a robust reaction of Cu-alloy/EPDM in the existence of TMSPM (coupling agent) as contrasted to without it (untreated).

3.6 Physical properties

The stress–strain curves are used to get a better sense of how physical properties improve with various concentrations of Cu-alloy loadings in all Cu-alloy/EPDM composites. According to Fig. 9, these bends are sensible to the concentration of the alloy cargos. Furthermore, for specified strain, each of filled systems exhibit higher stresses than

Fig. 9 Stress–strain curves of EPDM composites loaded with different content of untreated and treated Cu-alloy
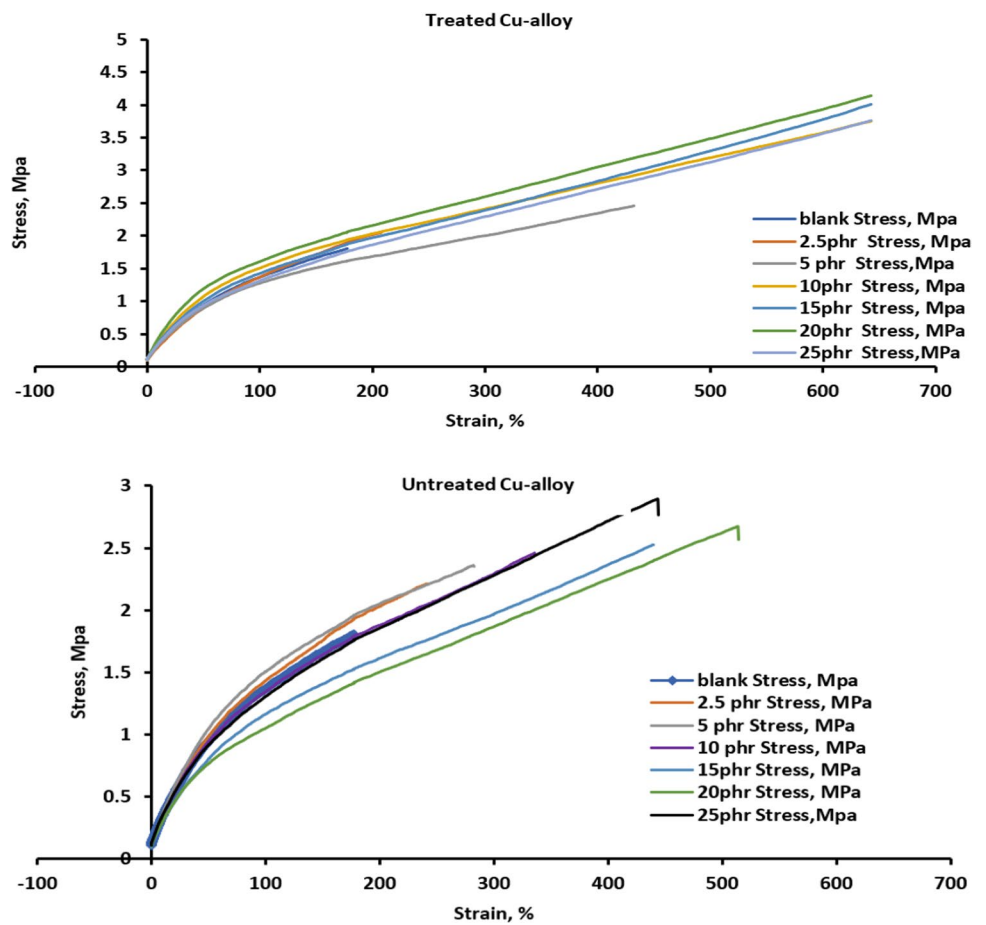

unfilled rubber. In comparison, failure stress values of 20 phr, 25 phr, and finally 15 phr of Cu-alloy were obtained in the existence or without of a conjugation factor. When the amount of Cu-based material was increased, it was discovered that there was an increasing trend of stress (tensile strength) and an increasing trend of strain (elongation). This is due to the fact that cross-link density (difference torque)

gradually decreases with increasing alloy loading (in this case). As more alloys were added, the compound became softer, increasing the degree of hardness and, as a result, tensile strength, while elongation gradually increased.

Evidence for the incorporation of Cu-alloy into EPDM rubber compounds can be noticed with or without of a conjugation factor (TMSPM), resulting in extra physical

Fig. 10 The relation between the strain energy of EPDM composites with Cu-alloy content
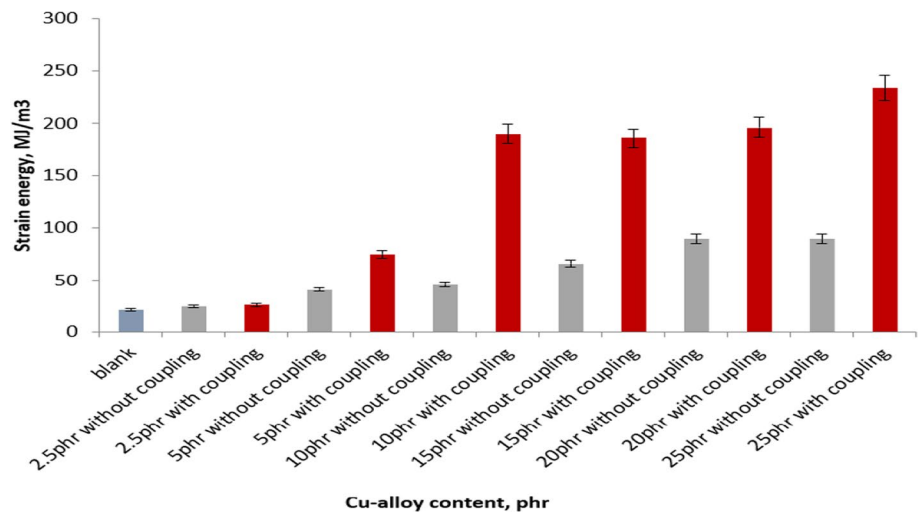
cross-links in the net structure of the composites. As a result, the energy absorbed per unit volume (EN) in deformed rubber composites is expected to increase, and can be written the energy absorbed as

$$EN = \oint \sigma(\varepsilon d\varepsilon), \tag{10}$$

where ε is the strain of function at stress σ; for that reason, higher energy absorption capacity is a signal of the greater the area under the stress–strain curves. Figure 10 displays that the strain energy of EPDM composites with dissimilar alloy concentrations in existence of a conjugation factor (TMSPM) was greater than that of those without. This indicates this compatibility of EPDM compounds and alloys with TMSPM has improved, particularly at 25 and 20 phr loadings. Therefore, Cu-alloy/EPDM that had not been treated had the smallest area under the stress–strain curves and, consequently, the lowest reduction power. On the other hand, adding 25 phr of alloy in existence of a conjugation factor showed the largest absorption energy compared to 25 phr without it. These results are in strong convention with the facts shown in Fig. 10, which demonstrates the rise in strain energy brought on by the addition of Cu-alloy to EPDM rubber compounds with TMSPM. It is well knowledge that without a coupling agent or strengthening metal, EPDM rubbers have rather weak physical and mechanical qualities.

The deformity based on the Mooney–Rivlin model was chosen toward imagine the technique of the reaction of alloy or filled rubber compounds to investigate the effect of Cu-alloy content at the mechanical properties of the EPDM compound. From the standpoint of thermodynamic flexibility or strain invariants, such as storable elastic energy, the "affine" deformation of a web of Gaussian series can be assumed identically [33, 34].

The Mooney–Rivlin relation [17] can explain the stress–strain behavior of EPDM rubber composites and by easy extension

$$\frac{\sigma}{2(\lambda - \lambda^{-2})} = C_1 + C_2\lambda^{-1}, \tag{11}$$

where C_1 and C_2 are constants mirroring specials of the webs, σ is the tensile stress, λ is the strain, and C_1 is an amount connected to the perfect elastic conduct [33], and C_2 expresses the divergence from it, whereas C_1 represents the non-Gaussian characteristics of the net and parameters of EPDM rubber compounds. It is important to note from Fig. 11 that in the range of investigated distortion, the all-filled compounds do not show any strain-result crystallization, but treated Cu-alloy/EPDM composites obtained a significant raise in stress, once again demonstrating the reaction

between the metal oxide (ZnO) and the inorganic stage in the presence of coupling agent.

On the side, the strain at which the rise happens reduced with the alloy filling. This result proposed the existence of several reactions among Cu-alloys and the EPDM chain. Either in the presence or absence of TMSPM, as the content of alloy rises, the C_2 value increases (Table 10). It has been discovered [33] that the Mooney–Rivlin constant, C_2, is related to the pliability of rubber series and intermolecular strengths. With an increase in the percentage of Cu-based alloy, this value rises (such as the filler–filler interplay). Due to the existence of upper chain tangle in the EPDM ingredients, the 25 phr treated Cu-alloy/EPDM is reported to have a riser C_2 value; higher chain tangle indicates better molecular plane blending. As a result, there is a strong correlation between the remark mechanical property fluctuation and the Mooney–Rivlin equation. For hardness, Cu-alloy/EPDM composites had about the same value of 57 (Shore A). Untreated Cu-alloy/EPDM had the lowest hardness due to Cu-alloy incompatibility with the EPDM matrix in the absence of a coupling agent (TMSPM). In general, the existence of Cu-alloys inside EPDM rubber template evidently decreases the hardness of the compounds. This phenomenon can be ascribing to the decrease in the cross-linking density due to non-adherence between filler and rubber mold, leading to softening rubber chain and hence allowing stretching when the strain is applied [17–35].

Table 10 shows that as the content of Cu-alloy in EPDM composite increases, then the number of fatigue cycles to failure increases, which may be ascribed to the power stored meanwhile the unsaturated dual bond of the pendant ethylene norbornene. And also, assigned to the increased of elasticity and decrease of cross-link density (ΔS) and as well reduce hardness of the composites. On the other hand, the addition of Cu-alloy influences fatigue in two reverse ways: increased the elongation at break tends to increase the fatigue strength; however, the enhanced hardness inclines to decrease it. Therefore, the fatigue resistance is a compromise between these two causes. Otherwise, the numeral series to failure showed higher values at presence treated Cu-alloy/EPDM composites than untreated composites. The tensile strength of composites without a coupling agent is higher in the previous study [8] than it is when a conjugation TMSPM is present. This could refer to introducing the TMSPM to the alloy/EPDM without first treating the surface of the alloy.

Scheme 2 shows some brief analysis of the relationship among the properties of the Cu-alloy/EPDM composites. These properties were obtained from different measurements, like ultrasonic, morphology, thermal gravimetric analysis, DSC, and rheological and physical properties. Good backing materials were obtained that had many effective properties.
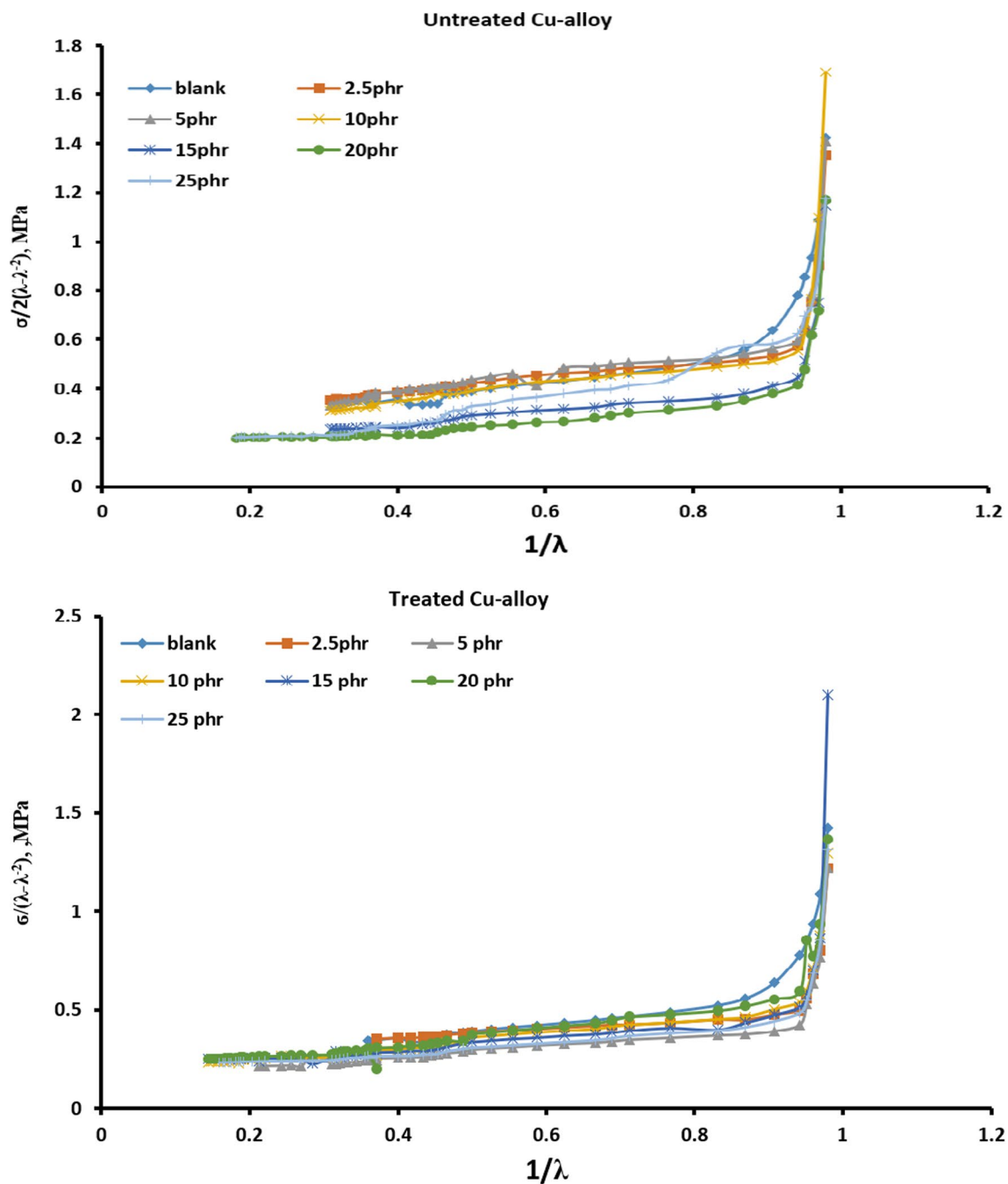
Fig. 11 Mooney–Rivlin plots for EPDM compounds filled with dissimilar content of untreated and treated Cu-alloy

4 Conclusion

Cu-alloy/EPDM composites were created successfully. Different concentrations of untreated and treated Cu–Al–Zn-alloy at 2.5, 5, 10, 15, and 20 phr were mixed with EPDM. Ultrasonic measurements like ultrasonic velocity, acoustic impedance, ultrasonic attenuation, and mechanical properties by ultrasonic allowed us to deduce that Cu-alloy/EPDM composites had good intermolecular arrangement, few gaps

and imperfections between molecules, good distribution of Cu-alloy in the EPDM matrix, and good mechanical properties. Morphology measurements (SEM pictures) ensured the uniform morphology of the composites, which had good thermal decomposition resistance (thermal stability) as a result of the thermal gravimetric analysis. DSC and rheological properties noted the high level of EPDM crystal perfection and proved that TMSPM was a good conjunction agent that improved Cu-alloy dispersion. The physical properties

Table 10 The physical properties for EPDM composites

Codes of sample	C_1, MPa	C_2, MPa	Hardness, shore A	No. of cycles to failure (fatigue life)
Blank (E0)	0.1211	0.4887	58	92×10^2
2.5phr untreated Cu-alloy (E1)	0.3295	0.2149	57	101×10^2
5phr untreated Cu-alloy (E2)	0.2853	0.2583	57	96×10^2
10phr untreated Cu-alloy (E3)	0.2789	0.25528	57	109×10^2
15phr untreated Cu-alloy (E4)	0.3164	0.2627	56	112×10^2
20phr untreated Cu-alloy (E5)	0.0412	0.3621	53	114×10^2
25phr untreated Cu-alloy (E6)	0.1318	0.3951	51	114×10^2
2.5phr treated Cu-alloy (E7)	0.2786	0.2261	59	99×10^2
5phr treated Cu-alloy (E8)	0.1783	0.2338	58	114×10^2
10phr treated Cu-alloy (E9)	0.242	0.251	57	123×10^2
15phr treated Cu-alloy (E10)	0.205	0.264	57	121×10^2
20phr treated Cu-alloy (E11)	0.193	0.366	53	119×10^2
25phr treated Cu-alloy (E12)	0.151	0.299	54	117×10^2

Scheme 2 Summary diagram for data analysis
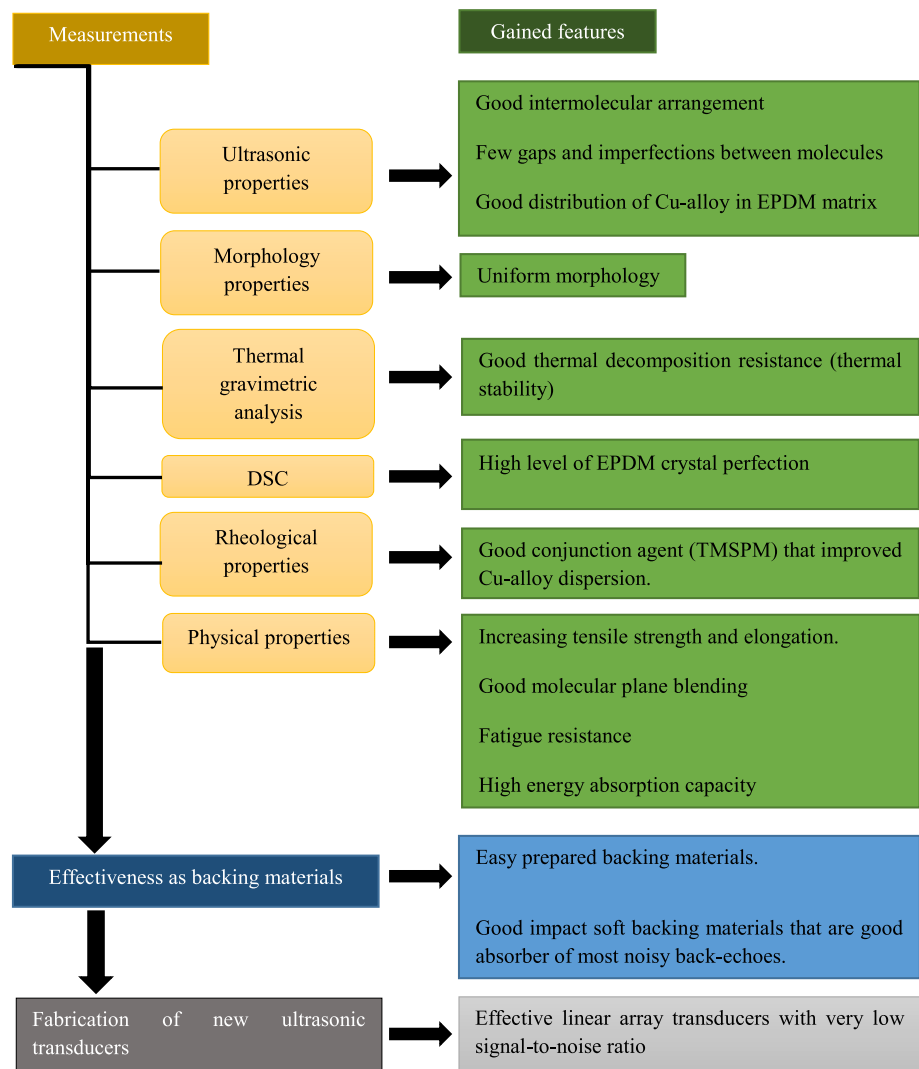
of the composites showed the increment of tensile strength and elongation, the improved molecular plane blending, the resistance to fatigue, and the increment of energy absorption capacity. In addition, the maximum density of the prepared EPDM composites did not exceed 1.058 kg/cm^3, which is sufficient to dampen the excess vibration of the piezoelectric material without being too dense to completely prevent it from moving. From all these composites' properties, we deduced that Cu-alloy/EPDM composites will be effective backing materials in ultrasonic array transducers. Thus, ten different linear ultrasonic-phased array transducers were fabricated. They contained Cu-alloy/EPDM composites (E0, E1, E2, E3, E4, E5, E6, E7, E8, E9, and E10). To assess the fabricated ultrasonic transducers, the signal-to-noise (S/N) ratio was measured. The lowest value of S/N is recorded when using a transducer with E6 backing composite, which is very effective in reducing noise echoes. In addition, E6 has the most consistent properties, such as acoustic impedance, ultrasonic attenuation coefficient, mechanical properties, etc., of the epoxy with tungsten backing material. The development of a good ultrasonic array transducer is of great benefit in medical diagnosis and in industrial applications.

Data Availability The data that support the findings of this study are available within the article.

Declarations

Conflict of interest There is no conflict of interest among the authors.

Ethical approval Not applicable.

References

1. X. Lei, H. Wirdelius, A. Rosell, Experimental validation and application of a phased array ultrasonic testing model on sound field optimization. J. Mod. phys **12**, 391–407 (2021). https://doi.org/10.4236/jmp.2021.124028

2. A. Abrar, D. Zhang, B. Su, T. Button, K.J. Kirk, S. Cochran, 1–3 connectivity piezoelectric ceramic-polymer composite transducers made with viscous polymer processing for high frequency ultrasound. Ultrasonics **42**(1–9), 479–484 (2004). https://doi.org/10.1016/j.ultras.2004.02.008

3. W. Lester, J. Schmerr, *Fundamentals of ultrasonic phased arrays: solid mechanics and its applications* (Springer International Publishing, Cham, 2015)

4. S.M. Al-Shomar, M.A.Y. Barakat, S.A. Mahmoud, A.A. Akl, Microstructure crystal imperfections and ultrasonic studies of sprayed nanosized $Cu_{2-x}S_xO$ and $Cu_{2-y}Cr_yO$ thin films. Dig. J. Nanomater. Biostruct. **13**(3), 885–901 (2018)

5. M.A.Y. Barakat, A.E.-A.A. El-Wakil, Preparation and characterization of EVA/ZnO composites as piezoelectric elements for ultrasonic transducers. Mater. Res. Express **8**, 105304 (2021). https://doi.org/10.1088/2053-1591/ac29fb

6. M. Toda, M. Thompson, Novel multi-layer polymer-metal structures for use in ultrasonic transducer impedance matching and backing absorber applications. IEEE Trans. Ultrason. Ferroelectr. Freq. Control. **57**, 2818–2827 (2010). https://doi.org/10.1109/TUFFC.2010.1755

7. Q. Miaomiao, Z. Bo, S. Yafei, Z. Yunhe, W. Xiaofeng, H. Weimin, Y. Zhu, Enhanced mechanical and dielectric properties of natural rubber using sustainable natural hybrid filler. Appl. Surf. Sci. Adv. **6**, 100171 (2021). https://doi.org/10.1016/j.apsadv.2021.100171

8. A. Nassar, D.S. Mahmoud, W.S. Mohamed, A.M. Moustafa, S.H. El-Sabbagh, Investigation of the structure, magnetic, rheological and mechanical properties of EPDM rubber/Cu-Al-Zn alloy composites. Egypt. J. Chem. **64**(12), 7377–7391 (2021). https://doi.org/10.21608/ejchem.2021.79716.3918

9. N.T. Nguyen, M. Lethiecq, B. Karlsson, F. Patat, Highly attenuative rubber modified epoxy for ultrasonic transducer backing applications. Ultrasonics **34**(6), 669–675 (1996). https://doi.org/10.1016/0041-624X(96)00064-9

10. S.M. Ji, J.H. Sung, C.Y. Park, J.S. Jeong, Phase-canceled backing structure for lightweight ultrasonic transducer. Sens. Actuators A Phys. **260**, 161–168 (2017). https://doi.org/10.1016/j.sna.2016.12.014

11. F. Dupont-Marillia, M. Jahazi, S. Lafreniere, P. Belanger, Design and optimization of a phased array transducer for ultrasonic inspection of large forged steel ingots. NDT E Int. **103**, 119–129 (2019). https://doi.org/10.1016/j.ndteint.2019.02.007

12. M.A.Y. Barakat, A.A. El-Wakil, Preparation of polyvinyl acetate composite as a new backing material for the manufacture of ultrasonic transducers. J. Mater. Res. **38**(3), 894–905 (2023). https://doi.org/10.1557/s43578-022-00881-y

13. M.A.Y. Barakat, Amelioration of ultrasonic transducer to study CuO doped thin films. Arch. Acoust **43**(3), 487 (2018). https://doi.org/10.24425/123920

14. S.M. Al-Shomar, M.A.Y. Barakat, A.W. Abdallah, Ellipsometric and ultrasonic studies of nano titanium dioxide specimens doped with Erbium. Mater. Res. Express **7**(10), 106413 (2020). https://doi.org/10.1088/2053-1591/abc0d0

15. M.A.Y. Barakat, A.E.-A.A. El-Wakil, E.H. Hasan, Modification of ultrasonic transducers to study crack propagation in vinyl polymers, supported by SEM technique. J. Vinyl Addit. Technol. **29**(1), 84 (2023). https://doi.org/10.1002/vnl.21945

16. F.M.L. Mekawey, E.H. Hasan, M. Barakat, Study of crack propagation in PMMA using ultrasonic technique. Polym. Plast. Technol. Eng. **46**(2), 151–156 (2007). https://doi.org/10.1080/03602550601152978

17. R.S. Rivlin, A.G. Thomas, Rupture of rubber. I. Characteristic energy for tearing. J. Polym. Sci. **10**(3), 291–318 (1953). https://doi.org/10.1002/pol.1953.120100303

18. El-Sabbagh, S.H., Ahmed, N.M., Turky, G.M., Selim, M.M.: Rubber nanocomposites with new core-shell metal oxides as nanofillers Ch. In Progress in Rubber Nanocomposites. In Progress in Rubber Nanocomposites. Edited by Sabu Thomas Hanna J. Maria, (2017) Woodhead Publishing is an imprint of Elsevier, pp. 249–283.

19. ASTM E114–15, Standard Practice for Ultrasonic Pulse-Echo Straight-Beam Contact Testing, ASTM International, West Conshohocken, PA (2015), www.astm.org.

20. E.M. Abou Hussein, M.A.Y. Barakat, Structural, physical and ultrasonic studies on bismuth borate glasses modified with Fe_2O_3 as promising radiation shielding materials. Mater. Chem. Phys. **290**, 126606 (2022). https://doi.org/10.1016/j.matchemphys.2022.126606

21. S.M. Al-shomar, M.A.Y. Barakat, S.A. Mahmoud, Modified ultrasonic technique to study Gd-doped ZnO films. Mapan J. Metrol. Soc. India **32**(2), 121–126 (2017). https://doi.org/10.1007/s12647-016-0199-8

22. Y. Ohara, K. Kikuchi, T. Tsuji, T. Mihara, Development of low-frequency phased array for imaging defects in concrete structures. Sensors **21**, 7012 (2021). https://doi.org/10.3390/s21217012

23. N. Hiremath, V. Kumar, N. Motahari, D. Shukla, An overview of acoustic impedance measurement techniques and future prospects. Metrology **1**(1), 17–38 (2021). https://doi.org/10.3390/metrology1010002

24. A.T. Fernandez, K.L. Gammelmark, J.J. Dahl, C.G. Keen, G.E. Trahey, Synthetic evaluation beamforming and image acquisition capabilities using an 8 x 128 1.75 D array. IEEE Trans. Ultrason. Ferroelectr. Freq. Control **50**(1), 40–57 (2003). https://doi.org/10.1109/tuffc.2003.1176524

25. N.T. Duong, J. Duclos, L. Bizet, P. Pareige, Relation between the ultrasonic attenuation and the porosity of a RTM composite plate. Phys. Proc. **70**, 554–557 (2015). https://doi.org/10.1016/j.phpro.2015.08.015

26. G. Maizza, A. Caporale, C. Polley, H. Seitz, Micro-macro relationship between microstructure, porosity, mechanical properties, and build mode parameters of a selective-electron-beam-melted Ti-6Al-4V alloy. Metals **9**(7), 786 (2019). https://doi.org/10.3390/met9070786

27. L.M. Zhang, M. Gao, G.Q. Luo, Z. Chen, Q. Shen, Preparation of tungsten-epoxy composites and FGMs with density gradient. Mater. Sci. Forum (2009). https://doi.org/10.4028/www.scientific.net/MSF.631-632.461

28. D. Hidayat, N.S. Syafei, B.M. Wibawa, M. Taufik, A. Bahtiar, Risdiana: metal-polymer composite as an acoustic attenuating material for ultrasonic transducers. Key Eng. Mater. **860**, 303–309 (2020). https://doi.org/10.4028/www.scientific.net/KEM.860.303

29. Y. Qiu, J. Liu, H. Yang, F. Gao, Y. Lu, R. Zhang, W. Cao, P. Hu, Graphene oxide-stimulated acoustic attenuating performance of tungsten-based epoxy films. J. Mater. Chem. C **3**, 10848 (2015). https://doi.org/10.1039/c5tc01347j

30. P.J. Howard, R.S. Gilmore, in *Review of progress in QNDE*. ed. by D.O. Thompson, D.E. Chimenti (Plenum Press, New York, 1994), pp.1069–1074

31. M. Bekhit, S.H. El Sabbagh, R.M. Mohamed, G.S. El Sayad, R. Sokary, Mechanical, thermal and antimicrobial properties of LLDPE/EVA/MMT/Ag nanocomposites films synthesized by gamma irradiation. J. Inorg. Organomet. Polym. **32**, 631–645 (2022). https://doi.org/10.1007/s10904-021-02137-4

32. A.A. Abdelsalam, S. Araby, S.H. El-Sabbagh, A. Abdelmoneim, M.A. Hassan, Effect of carbon black loading on mechanical and rheological properties of natural rubber/styrene-butadiene rubber/nitrile butadiene rubber blends. J. Thermoplast. Compos. Mater. **34**, 4 (2019). https://doi.org/10.1177/0892705719844556

33. D.S. Mahmoud, A.A. Said, A.E. Abd El-Kader, S.H. El-Sabbagh, Enhanced physico mechanical performance of nitrile rubber composites by utilizing eco-friendly natural oil as a plasticizer. J. Vinyl. Addit. Technol. **28**(4), 894–906 (2022). https://doi.org/10.1002/vnl.21936906MAHMOUDETAL

34. C. Yu, J. Mark, The use of compression measurements to study stress–strain relationships and the volume dependence of the elastic free energy of a polymer network. Polym. J. **7**, 101–107 (1975). https://doi.org/10.1295/polymj.7.101

35. A.I. Al-Ghonamy, M.A. Barakat, Upgrading of acrylonitrile-butadiene copolymer properties using natural rubber-graft-*N*-(4-aminodiphenylether) acrylamide. J. Appl. Polym. **118**(4), 2202–2207 (2010). https://doi.org/10.1002/app.32571